CRYSTAL GROWTH & DESIGN

pubs.acs.org/crystal

Article

# Chiral Resolution of Mandelic Acid through Preferential Cocrystallization with Nefiracetam

Xavier Buol, Camila Caro Garrido, Koen Robeyns, Nikolay Tumanov, Laurent Collard, Johan Wouters, and Tom Leyssens*

Cite This: *Cryst. Growth Des.* 2020, 20, 7979−7988

Read Online

ACCESS | Metrics & More | Article Recommendations | Supporting Information

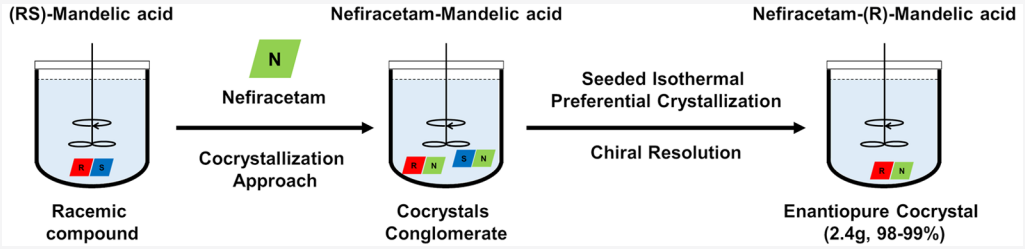


**ABSTRACT:** In this paper, we identified a cocrystal conglomerate of mandelic acid using a drug compound as a coformer. We then developed a chiral resolution process based on preferential cocrystallization. Several versions of such a process were explored and optimized, leading to a successful resolution of mandelic acid, evidencing the efficiency of our system. Excellent enantiopurity (98−99%) was obtained with a process that can run for multiple cycles.

## INTRODUCTION

A chiral molecule exists in two nonsuperimposable configuration images called enantiomers. These enantiomers exhibit identical physicochemical properties in an achiral environment.[1,2] When these enantiomers are placed in a chiral surrounding, differences in their behavior can occur.[3] The human body typically shows such a chiral setting, often reflected in differences in therapeutic effect between two enantiomers of pharmaceutically active compounds. Whereas one enantiomer shows a desired effect (eutomer), the other enantiomer (distomer) shows a similar, no, or a negative effect, as is the case e.g. for thalidomide.[4] It is therefore recommended to market new chiral drugs containing only the desired enantiomer.[5] It is thus important during drug development to develop a production process that eventually leads to the eutomer.[3,6,7] Two approaches are common. The first approach is to develop a synthetic pathway for a single enantiomer through asymmetric synthesis. Asymmetric synthesis groups different approaches such as enantioselective synthesis, the chiral pool,[8] the use of chiral auxiliaries,[9] and asymmetric catalysis.[10,11] However, this pathway is not always feasible or cost-effective. An alternative, common approach is to resolve both enantiomers from a racemic mixture. Common resolution methods are kinetic resolution,[12] chiral chromatography,[13] diastereoisomeric salt formation,[14] resolution by enantiospecific[15] or diastereomeric cocrystallization[16] and preferential crystallization (PC),[17,18] with the last three methods being crystallization-based processes. Preferential crystallization or resolution by entrainment, however, can only be performed when the compound crystallizes as a conglomerate (defined as *a physical mixture of mirror-image crystalline phases exhibiting symmetrical enantiomeric excesses*[17]) which only occurs in less than 10% of cases.[19,20] To increase the potential of PC, a recent tactic focuses on converting a racemic compound into a conglomerate using a crystal engineering approach.[21] Typically, salt[22] formation or the use of solvates[23] is commonly encountered for this transformation. Recently cocrystallization[24−27] has also been explored as an interesting alternative. Harfouche et al.[28] then went beyond mere identification of a cocrystal conglomerate, showing the first application of PC to the racemic pharmaceutical substance proxyphylline through the conversion of the racemic compound into a monohydrate conglomerate cocrystal. A purity of 91.6% in favor of the desired enantiomer was achieved in a single entrainment step.

In this work, we also use preferential cocrystallization, being the first to propose resolution of racemic mandelic acid through preferential crystallization. To do so, the racemic compound of mandelic acid is transformed into a conglomerate, cocrystallizing this latter species with nefiracetam,[29−32] an achiral nootropic drug molecule (Figure 1). Mandelic acid,

**Received:** September 7, 2020
**Revised:** October 29, 2020
**Published:** November 9, 2020







https://dx.doi.org/10.1021/acs.cgd.0c01236
*Cryst. Growth Des.* 2020, 20, 7979−7988

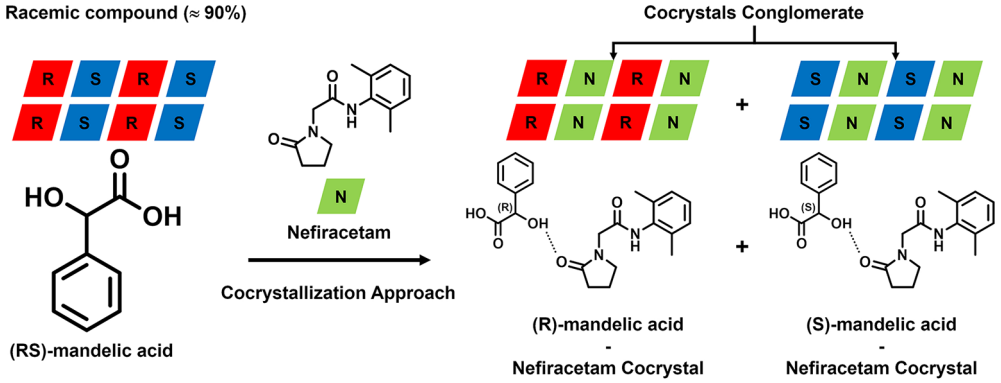


**Figure 1.** Cocrystallization approach to convert the racemic compound of mandelic acid into a nefiracetam conglomerate cocrystal.

which is resolved by diastereoisomeric salt formation,[33] is commonly used in the pharmaceutical industry due to its analgesic, antirheumatic, and spasmolytic effects, and its enantiopure forms are widely used as resolving agents.[34,35] We present here detailed evidence of this dual-drug conglomerate formation and then subsequently develop a preferential crystallization for the resolution of mandelic acid using different approaches such as a seeded isothermal preferential crystallization (SIPC) and a seeded polythermal preferential crystallization (S3PC).[36−38] We were able to develop a cyclic process in which we resolved up to at least 2.4 g of mandelic acid, with an enantiopurity of 98−99%, being the first to report mandelic acid resolution using preferential cocrystallization.

## MATERIALS AND METHODS

**Materials.** Nefiracetam (N) was sourced from Xiamen Top Health. All solvents used are commercially available from VWR. Solvents were used as received without any additional purification. Nefiracetam was purified by slurrying the compound overnight in ethyl acetate at room temperature, after which the suspension was filtered and dried. (*RS*)-Mandelic acid (RSMA, >99%), (*S*)-Mandelic acid (SMA, >99%), and (*R*)-mandelic acid (RMA, > 99%) were purchased respectively from ACROS, TCI, and Sigma-Aldrich and used as received.

**Methods.** *Cocrystal Conglomerate Screening.* Cocrystal conglomerate screening was performed by liquid-assisted grinding (LAG), using a Retsch Mixer Mill MM 400 equipped with two grinding jars each able to contain five 2 mL Eppendorf tubes. Each tube was filled with equimolar amounts (±0.3 mmol) of nefiracetam and mandelic acid (RSMA, RMA, or SMA), four small stainless-steel beads, and 10 μL of methanol. Grinding was then performed at 30 Hz for 90 min.

*Single-Crystal Growth.* Single-crystal growth was achieved through evaporative crystallization experiments, performed by preparing undersaturated solutions of equimolar amounts (0.1 mmol) of nefiracetam and mandelic acid (RSMA and RMA) in a suitable amount of solvent. The solutions were then left to evaporate slowly (from 3 to 7 days) at room temperature and the crystals retrieved once they appeared. Solvents tried included ethanol, methanol, acetonitrile (MeCN), tetrahydrofuran (THF), acetone, dichloromethane, chloroform, ethyl acetate (EtOAc), methyl acetate, diethyl ether, 2-propanol, and water. Crystals of NRMA (1:1 nefiracetam−(*R*)-mandelic acid cocrystal) suitable for SCXRD were obtained from ethyl acetate.

*Congruency Experiments.* Congruency experiments were achieved through slurry crystallization. Slurrying experiments were performed by preparing equimolar suspensions (0.3 mmol) of nefiracetam and mandelic acid (RSMA, RMA, or SMA) in the aforementioned solvents. The suspensions were stirred at 700 rpm for 3 days at 25 °C in sealed vials using an HLC Cooling Thermomixer. After 2 h of stirring, each vial was seeded with all possible solid forms (parent compounds and the enantiopure cocrystal or cocrystal conglomerate). Once equilibrium was reached, the powders were filtered, washed, dried, and analyzed using XRPD.

Enantiopure seeds (NRMA and NSMA) production were upscaled to ±16 g in ethyl acetate. To do so, equimolar amounts of nefiracetam (12.00 g) and RMA or alternatively SMA (7.41 g) were placed in a reactor vessel filled with ethyl acetate (100 mL). The suspension was stirred (ca. 300 rpm) for 48 h at 23 °C, after which the suspension was filtered and the solids were washed with ethyl acetate and dried. This material was used as the seeding material. NRSMA (1:1 nefiracetam−(*RS*)-mandelic acid cocrystal conglomerate) was upscaled to ±65 g in ethyl acetate as well using a 1 L Reactor-Ready Lab Reactor from Radleys and the material used for the PC process. Nefiracetam (50.00 g) and (*RS*)-mandelic acid (30.89 g) were added to 750 mL of ethyl acetate, and the mixture was stirred at 23 °C. After a 2 day time period, the suspension was filtered and the solid recovered as mentioned above.

*Powder X-ray Diffraction (XRPD).* Powder X-ray diffraction (XRPD) data were collected on a PANalytical Bragg−Brentano diffractometer, using Ni-filtered Cu K$\alpha$ ($\lambda$ = 1.54179 Å) at 45 kV and 30 mA with a X'Celerator detector. Each sample was analyzed between 4 and 40° in 2$\theta$ with a step size of ca. 0.0167° and a total scan time of 6 min 42 s.

*Single-Crystal X-ray Diffraction (SCXRD).* Single-crystal X-ray diffraction (SCXRD) was performed on a suitable single crystal of NRMA and analyzed using an Oxford Diffracton Gemini R Ultra diffractometer (Ruby CCD detector using Cu K$\alpha$ radiation). Data reduction was carried out using the CrystAlisPRO software package.[39] The resolution and refinement by full-matrix least squares were carried out using respectively SHELXT and SHELX-2018/3.[40] Non-hydrogen atoms were refined anisotropically; H atoms were added in calculated positions and allowed to ride on the parent atoms, with isotropic displacement factors set to 1.2$U_{eq}$ of the parent atoms ($U_{iso}$(H) = 1.5$U_{eq}$(C) for methyl). The H atoms of the methyl groups were allowed to undergo free rotation about the local 3-fold axis. Symmetry analysis and validation were carried out using PLATON.[41] Figures were drawn using the molecular visualization software Mercury v4.1.3.[42] CCDC 2023975 and 2032987 include the supplementary crystallographic data and can be downloaded free of charge from The Cambridge Crystallographic Data Centre via www.ccdc.cam.ac.uk/structures.

*Differential Scanning Calorimetry (DSC).* Differential scanning calorimetry (DSC) experiments were performed from 25 to 175 °C, with a scanning rate of 5 °C min$^{-1}$ on a TA Instruments DSC2500 apparatus. The heating rate was increased to 10 °C min$^{-1}$ for some of the routine analyses. The solid phases were weighed (6−7 mg) in aluminum pans with perforated lids. The purge gas was nitrogen, with a flow rate of 50 mL min$^{-1}$. Indium was used as a reference prior to the analyses. The data were treated using TA Instruments TRIOS v5.1.0.46403 software.

*Thermogravimetric Analysis (TGA).* Thermogravimetric analysis (TGA) was performed on a Mettler Toledo TGA-STDA 851e


https://dx.doi.org/10.1021/acs.cgd.0c01236
Cryst. Growth Des. 2020, 20, 7979−7988

instrument, varying the temperature from 25 to 400 °C, at a scanning rate of 10 °C $min^{-1}$. Solid samples (7−10 mg) were placed in aluminum oxide crucibles, and nitrogen was used as purge gas with a flow rate of 50 mL $min^{-1}$. Data were treated with the STARe 12.12 software.

*Solubility Curves.* Solubility curves of RSNMA and RNMA were obtained by weighing the solids in increasing amounts in 1.5 mL vials, topped with 1 mL of acetonitrile and then sealed. Each vial was equipped with a stirring magnet. A heating−cooling cycle was then applied to the vials from 0 to 60 °C with a heating/cooling rate of 0.1 °C $min^{-1}$ and with a continuous stirring of ca. 700 rpm using a Crystal 16 crystallization system (Technobis). The turbidity was continuously monitored, allowing identification of clear (solubility) and cloud (nucleation) points. The software Crystal Clear 1.0.1.614 was used to process the data and to construct solubility and crystallization curves.

*Binary Phase Diagram (BPD).* A binary phase diagram (BPD) was built by plotting the onset and endset of melting obtained from the DSC data performed on a set of 11 samples. Samples were prepared by weighing RMA and SMA in different molar fractions (with $n_{tot}$ = 0.244 mmol) and a constant amount of nefiracetam ($n$ = 0.244 mmol) in 2 mL Eppendorf tubes. A classical LAG method as described previously was applied on the samples.

*Chiral High-Performance Liquid Chromatography (cHPLC).* Calibration lines for HPLC were constructed to dose RMA by correlating the concentration and the area under the curve (AUC) with a linear equation. The samples were first diluted using a mixture of ethanol and isohexane (1:1) as diluent (dilution factor from 1 to 0.25). The concentrations were dosed using the following HPLC parameters: device, Waters Alliance 2695; column, Daicel Chiralpak IC, 4.6 × 250 mm, 5 μm; detector, Waters 996 Photodiode Array Detector (PDA) (Max Plot); $T$ = 25 °C; injection volume, 10 μL; flow, 1 mL/min; mobile phase, 95% isohexane, 5% 2-propanol, 0.1% trifluoroacetic acid; equilibration time of 30 min and wash of the column with isohexane/ethanol (80/20) after three sample runs; stop time, 30 min. The calibration line is reported in the Figure S10 in the Supporting Information. Slight changes in the mobile phase (iHex, IPA, and TFA) composition strongly affect the elutio,n and therefore retention times may vary from one experiment to another.

*Reverse High-Performance Liquid Chromatography (rHPLC).* Calibration lines for high-performance liquid chromatography (HPLC) were first built to dose nefiracetam by correlating the area under the curve (AUC) and the concentration prepared with a linear equation. The filtered liquid phase from the NRSMA suspensions in MeCN were first diluted 4000× using a 1/1 v/v acetonitrile/Milli-Q water diluent. Nefiracetam concentrations were dosed using the following HPLC parameters: device, Waters Alliance 2695; column, Waters Sunfire $C_{18}$, 4.6 × 100 mm, 3.5 μm; detector, PDA 2998 (Max Plot); $T$ = 40 °C; injection volume, 10 μL; flow, 1.2 mL $min^{-1}$; mobile phase A, $H_2O$ + 0.1% $H_3PO_4$; mobile phase B, $CH_3CN$ + 0.1% $H_3PO_4$; gradient, 0 min → 30% B; 0.5 min → 30% B; 4.5 min → 90% B; 6.5 min → 90% B; stop time, 15 min. The NRSMA solubility was extrapolated from the nefiracetam concentration. The calibration lines are reported in Figures S14−S16 in the Supporting Information.

*Ternary Phase Diagram (TPD).* An isothermal section of the ternary phase diagram (TPD) at 23 °C in MeCN of the NRSMA conglomerate was represented using the software ProSim Ternary Diagram. To do so, 11 slurry samples were prepared by weighing RMA and SMA in different molar fractions (with $n_{tot}$ = 0.5 mmol) and an equimolar and constant amount of nefiracetam ($n$ = 0.5 mmol) in a constant volume of 0.5 mL of acetonitrile. The vials were then sealed and the contents stirred at 700 rpm for 3 days at 23 °C. Once equilibrium was reached, the saturated mother liquors were recovered by filtration and 20 μL of each liquid phase was weighed ($m_{tot}$) and diluted 250-fold, using a 1/1 mixture of isohexane and ethanol. A 20 μL portion from each dilution was injected in the chiral HPLC. The aforementioned calibration line yielded the concentration and thus the molar fractions of NRMA and/or NSMA. The molar amount of nefiracetam was equivalent to the total amount of mandelic acid in solution, and the molar fraction of the solvent was deduced by mass balance.

*Preferential Crystallization Process.* The preferential crystallization experiments in a single (SIPC and S3PC) vessel were performed with an EasyMax 102 Advanced Workstation (Mettler Toledo), equipped with two jacketed 100 mL flasks, with stirring and temperature control (resolution 0.1 °C). To create a saturated solution for the SIPC mode, a NRSMA conglomerate suspension was prepared at temperature T1. Once the equilibrium (24 h is considered here) was reached, the suspension was filtered and the filtrate saturated at temperature T1 and rapidly cooled to the crystallization temperature T2 (without any spontaneous nucleation observable). Homochiral seeds of NRMA were then placed in the crystallizer with stirring reduced to 150 rpm, allowing the preferential crystallization to set in. The batch crystallization process was stopped after a given time $t_{end}$. The solid phase was recovered through filtration and washed with cold ethyl acetate. In the case of an S3PC mode, the saturated solution was seeded at T1 and a slow cooling ramp (cf. Table 2) was applied until T2.

*Liquid-Phase Sampling.* For a kinetic follow-up of the process 250 μL of the liquid phase was sampled every 10 min, using a 1 mL syringe with a microfilter (porosity 0.2 μm) to follow the ee over time.

*Solid-Phase Sampling.* For a kinetic follow-up of the process 2 mL of the liquid phase containing solid particles was sampled every 10 min, using a 2 mL syringe. The liquid phase was then filtered and the solid recovered. No washing was applied.

## RESULTS AND DISCUSSION

**1:1 Nefiracetam−(*RS*)-Mandelic Acid Cocrystal Conglomerate (NRSMA).** In our previous work,[31] we set out to enhance nefiracetam solubility through cocrystallization. A cocrystal screen was performed, choosing potential coformers based on supramolecular synthons. As nefiracetam exhibits an amide group, carboxylic acids were the obvious choice, as the acid−amide heterosynthon is often encountered in cocrystals. Grinding a 1/1 mixture of (*RS*)-mandelic acid with nefiracetam led to the formation of a new solid phase, as shown in Figure 2, with the ground product exhibiting easily

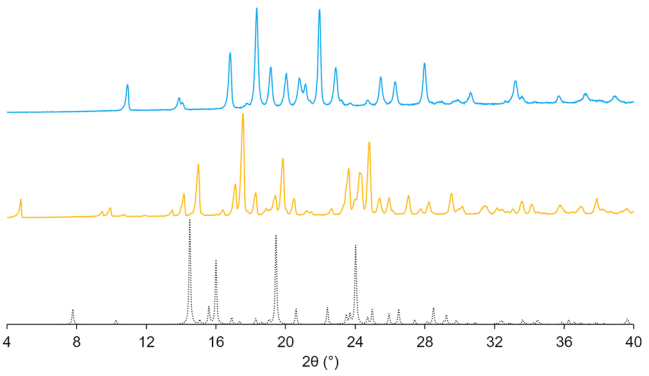


**Figure 2.** Simulated diffraction patterns (dashed line) and experimental powders (solid line) of nefiracetam FI (black), 1:1 nefiracetam−(*RS*)-mandelic acid ground product (yellow), and (*RS*)-mandelic acid (light blue).

observable peaks (at 2$\theta$ = 4.71, 9.43, 9.93, 14.09, 14.96, and 17.46°) not belonging to the parent compounds. Furthermore, the characteristic peaks of nefiracetam and (*RS*)-mandelic acid were no longer present in the ground material.

Single crystals were then grown to confirm cocrystal formation starting from a nefiracetam/mandelic acid racemate (1:1) undersaturated solution in ethyl acetate through evaporative crystallization. Single-crystal X-ray diffraction


https://dx.doi.org/10.1021/acs.cgd.0c01236
Cryst. Growth Des. 2020, 20, 7979−7988

(SCXRD) measurements were carried out using Cu radiation, allowing full characterization of the crystal and determination of the absolute configuration of the crystal. The crystal presented a cubelike shape and was shown to be a 1:1 cocrystal of nefiracetam and (*R*)-mandelic acid in the chiral orthorhombic space group $P2_12_12_1$. The crystal was harvested from a mixture containing both (*R*)- and (*S*)-mandelic acid, and the absolute configuration was unambiguously assigned by analysis of the anomalous difference; the refined Flack parameter was −0.03(10). Further SCXRD experiments on a single crystal grown by evaporation from a nefiracetam−(*R*)-mandelic acid solution resulted in a similar Flack parameter (−0.07(6)). The main crystallographic and refinement parameters are summarized in Table S1 in the Supporting Information. The molecules of nefiracetam are linked together via strong intermolecular amide−amide hydrogen bonds (O2···H2−N2, 2.834(2) Å, 171(2)°), between the −NH moiety of the amide group and the carbonyl moiety of the amide group of a neighboring molecule (Figure 3A). This arrangement leads to a $C_1^1(4)$ hydrogen bonding pattern according to the Etter graph notation.[43] Each mandelic acid molecule is shown to share two hydrogen bonds (Figure 3B). A first hydrogen bond is formed with another mandelic acid molecule, between the carbonyl moiety of the carboxylic acid group of one molecule and the hydroxyl group of the other (O4···H5−O5, 2.762(3) Å, 16(4)°). The second hydrogen bond is found between mandelic acid and a nefiracetam molecule, with the −OH moiety of the carboxylic acid group of mandelic acid linking to the carbonyl moiety of the γ-lactam ring (O1···H3−O3, 2.601(3) Å, 162(3)°). These hydrogen bonding patterns can be described by a $C_1^1(4)$ infinite chain pattern for the intermolecular hydrogen bond O4···H5−O5 and a $D_1^1(2)$ finite pattern for the hydrogen bond O1···H3−O3 between the mandelic acid and nefiracetam molecules. To allow for both hydrogen-bonding patterns, all mandelic acid molecules must have the same absolute configuration. Overall (Figure 3C) sheets of nefiracetam molecules are present thanks to the amide−amide interactions. These sheets are linked together by dimeric layers of mandelic acid molecules. The orientation of the hydrogen atom on the asymmetric carbon alternates from one layer to the other. Such an orientation does not allow for mandelic acid molecules of opposite handedness.

As the initial enantiopure nefiracetam−(*R*)-mandelic acid single crystal was grown from a racemic solution, conglomerate formation was suspected. Furthermore, the simulated XRPD pattern from this structure fits with that obtained by grinding of racemic mandelic acid with nefiracetam. To confirm conglomerate formation, slurry crystallization experiments were performed in ethyl acetate using racemic as well as enantiopure mandelic acid and an equimolar amount of nefiracetam. The obtained patterns are shown in Figure 4. XRPD does not indicate the parent compounds to be present in the isolated solids, indicating a congruent behavior of the cocrystal in this solvent. Furthermore, XRPD patterns of the racemic and enantiopure slurry products perfectly overlap and correspond more to the simulated pattern of the enantiopure single crystal.

Further proof of conglomerate formation was given by hand picking a single cubelike cocrystal obtained from a nefiracetam−(*RS*)-mandelic acid cooling experiment and analyzing this latter crystal by chiral HPLC. In parallel, the overall powder obtained upon full evaporation of an under-

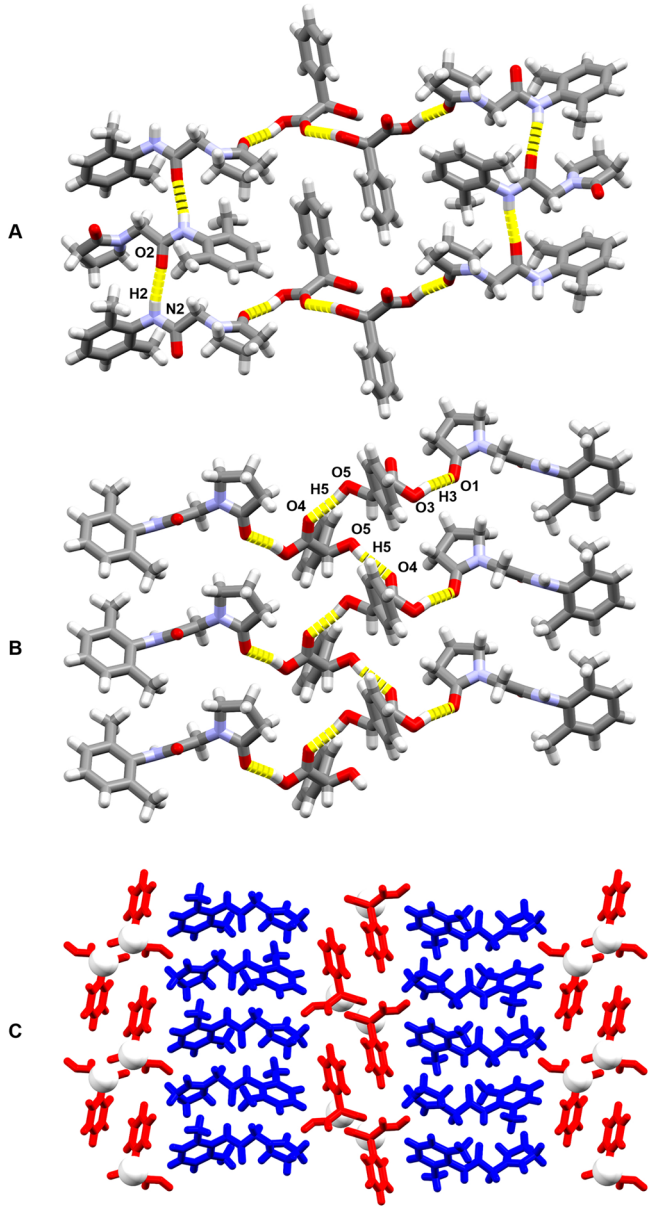


**Figure 3.** Views along the (A) *a* axis and (B) *b* axis showing the hydrogen bond network in the NRMA cocrystal. Atoms involved in the hydrogen bond pattern description are labeled. Wide view along the *a* axis (C) of the NRMA cocrystal. Nefiracetam and (*R*)-mandelic acid are respectively colored in blue and red. The hydrogens on the asymmetric carbon of (*R*)-mandelic acid are highlighted using a space-filling representation.

saturated nefiracetam−(*RS*)-mandelic acid solution was also tested as a reference. As expected, the latter powder shows two distinct peaks, at retention times of 9.403 min (RMA) and 10.189 min (SMA) (Figure 5A), with a 50:50 *R*:*S* composition. For the former crystal, however, a single retention peak is observed (Figure 5B), confirming the enantiopurity of the crystals obtained.[50]

As a final proof of conglomerate formation, a binary melting diagram was constructed. Figure 6 shows a diagram typical of a conglomerate with a single eutectic melt at the racemic composition. NRMA (and NSMA) shows a melting temperature at 114.9 °C, whereas the eutectic melt is located at 98.4 °C (Figure 7). The DSC data required for the diagram


https://dx.doi.org/10.1021/acs.cgd.0c01236
Cryst. Growth Des. 2020, 20, 7979−7988

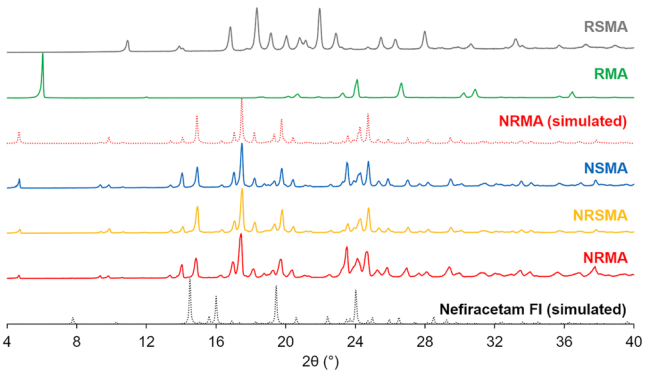


**Figure 4.** Simulated diffraction patterns (dashed lines) and experimental powder patterns (solid lines) of nefiracetam FI simulated (black), 1:1 nefiracetam−(*R*)-mandelic acid (NRMA, red), 1:1 nefiracetam−(*RS*)-mandelic acid (NRSMA, yellow), 1:1 nefiracetam−(*S*)-mandelic acid (NSMA, blue), 1:1 nefiracetam−(*R*)-mandelic acid simulated (NRMA simulated, red), (*R*)-mandelic acid (RMA, green), and (*RS*)-mandelic acid (RSMA, gray) from slurry experiments in ethyl acetate.

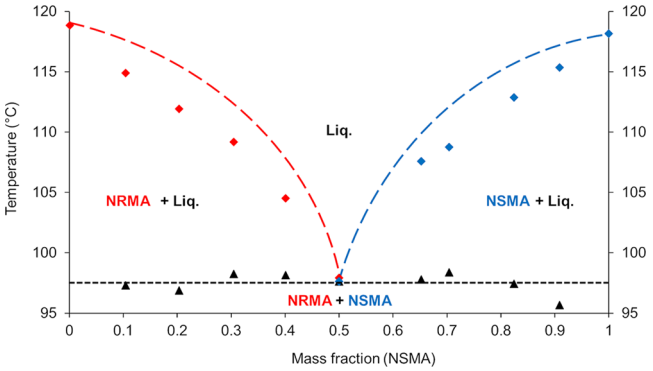


**Figure 6.** Binary melting phase diagram of the nefiracetam−(*RS*)-mandelic acid system. The diagram is typical of a conglomerate-forming system.

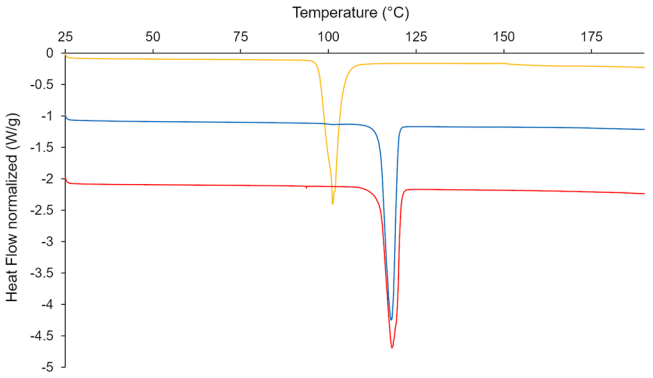


**Figure 7.** DSC curves of NRSMA bulk material (yellow), NSMA (blue), and NRMA (red).

construction are presented in Table S2 and Figure S1 in the Supporting Information. In addition, a TGA analysis (Figure S2 in the Supporting Information) of NRMA does not show any degradation prior to 175 °C, implying that degradation was overlapping with the calorimetric measurements needed to construct the phase diagram. Integration of both peaks shows an enthalpy of fusion $\Delta H_f$ of about 40.3 kJ mol$^{-1}$ for NRSMA and 48.6 kJ mol$^{-1}$ for NRMA. The negative value of the difference in enthalpy of fusion ($\Delta\Delta H_f$ is −8.3 kJ mol$^{-1}$) is typical for a conglomerate-forming system.[44] The theoretical eutectic may be also extrapolated by the Shröder−van Laar equation using the melting point and the enthalpy of fusion of the enantiopure form. The calculated value of 97.8 °C fits with that determined by DSC (98.4 °C).[45−47] A ternary phase diagram in MeCN at 23 °C is also presented in Table S3 and Figures S5−S9 in the Supporting Information, once more evidencing the conglomerate behavior of our system.

**Chiral Resolution of Mandelic Acid by Preferential Cocrystallization.** We then set out to resolve mandelic acid

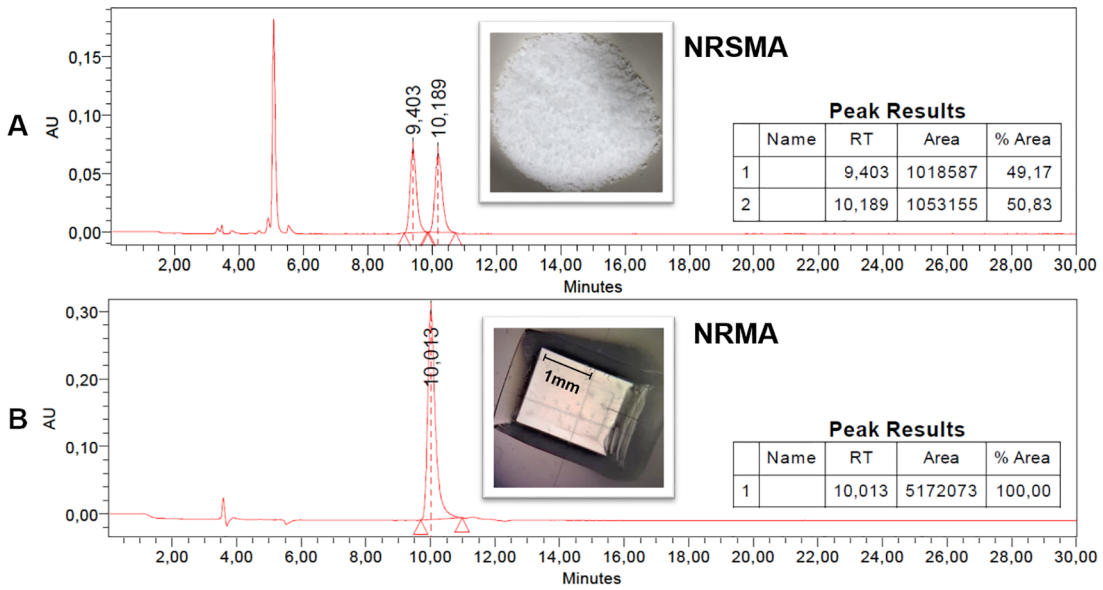


**Figure 5.** cHPLC chromatograms of (A) NRSMA bulk material and (B) a single crystal from a cooling experiment of NRSMA in ethyl acetate. Pictures of the NRSMA bulk material as well as the NRMA single crystal are also provided. The full chromatograms are presented in Figure S4 in the Supporting Information.



https://dx.doi.org/10.1021/acs.cgd.0c01236
Cryst. Growth Des. 2020, 20, 7979−7988

through a preferential cocrystallization process, which up to now has only been developed in one specific case.[28] In comparison to classical preferential crystallization, preferential cocrystallization is faced not only with the risk of having both enantiomers crystallizing out but also with that of a parent compound crystallizing out instead of the cocrystal. An ideal solvent, therefore, not only needs to show a wide metastable zone but also needs to lead to a congruent system. Congruency experiments were performed in acetonitrile, chloroform, dichloromethane, diethyl ether, ethanol, water, 2-propanol, tetrahydrofuran, and ethyl acetate. Results are presented in the Supporting Information and reveal that our system is congruent in most of the solvents with the exception of THF, 2-propanol, and water. Preferential crystallization trials in ethyl acetate led to spontaneous nucleation of nefiracetam upon seeding (Supporting Information), and this solvent could therefore not be used for further development. Out of the remaining solvents, acetonitrile was selected for further development. Solubility curves (Figure 8) of both the

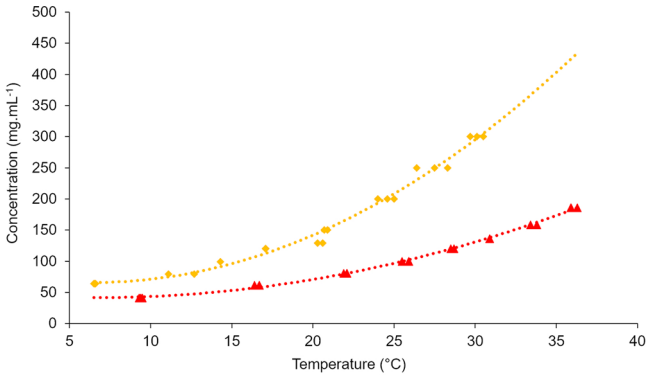


**Figure 8.** Solubility curves of NRSMA (yellow) and NRMA (red) in MeCN.

nefiracetam−mandelic acid conglomerate (NRSMA) and the enantiopure cocrystal (NRMA or NSMA) were established. The cocrystal responds to Meyerhoffer's double-solubility rule:[48] e.g., at 23 °C the solubility of the NRSMA conglomerate is 180.15 mg $mL^{-1}$ whereas that of the enantiopure cocrystal is 88.53 mg $mL^{-1}$. Furthermore, the rapid increase in solubility from 20 °C onward already highlights the fact that any crystallization process is ideally performed with filtration below this temperature to avoid important losses in the mother liquor. With use of a van't Hoff plot (Figure S3) the enthalpy $\Delta H_{diss}$ and entropy $\Delta S_{diss}$ of dissolution of NRMA at 25 °C were determined to be 81.8 kJ $mol^{-1}$ and 251.2 J $mol^{-1}$ $K^{-1}$, respectively. The respective values for the conglomerate are to 94.5 kJ $mol^{-1}$ and 305.9 J $mol^{-1}$ $K^{-1}$.

We then attempted to resolve the racemate using a conventional single-batch preferential crystallization (see Material and Methods), more precisely in a seeded isothermal preferential crystallization (SIPC) mode. A series of 15 experiments were performed with the most representative ones shown in Table 1; the remaining experiments are placed in Tables S4 and S5 in the Supporting Information.

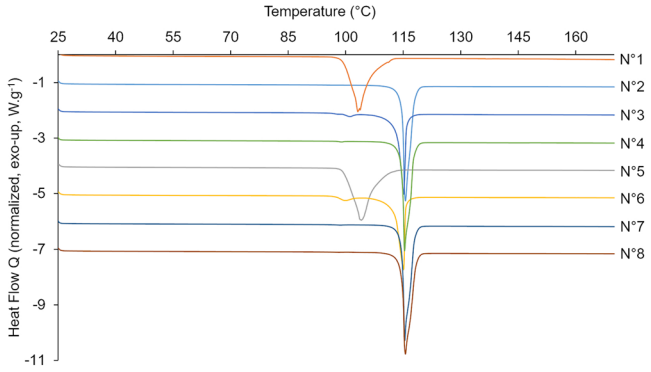


**Figure 9.** DSC analyses performed on the solid outcomes of trials 1−8.

DSC (Figure 9) and chiral HPLC (Figure 10) analyses were performed on all solids recovered. The resolution index (RI) allows evaluating the efficiency of the separation according eq 1 with $m_{recovered}^{NRMA}$ being the total mass of material recovered corrected using the enantiopurity[3] to determine the amount of *R* enantiomer. The enantiopurity is given by chiral HPLC (% area). An efficient resolution ideally has an RI value superior to 2.[3] The yield ($\gamma$, eq 3) reflects the amount of enantiopure cocrystal coming out vs the maximum amount that can be crystallized according to the solubility data (Figure 8). The productivity ($Pr^{NRMA}(t)$eq 2) of the process is then defined as the amount of NRMA that crystallized out per unit time,[38] in comparison to the maximum amount of NRMA that can potentially crystallize out. The productivity is only estimated when the purity is over 90%. The supersaturation ratio $\beta_{mass}$ (eq 4) is obtained by considering the solubility at T1-$m_{NRSMA(T1)}$ and T2-$m_{NRSMA(T2)}$, respectively, being the masses required to saturate the solution at T1 and T2.

$$RI = \frac{m_{recovered}^{NRMA} - m_{seed}}{m_{seed}} \quad (1)$$

**Table 1. Process Parameters and Results of the Eight Most Representative SIPC Trials**[a]

| no. | PC mode | *V* (mL) | T1 (°C) | T2 (°C) | cooling rate (°C $min^{-1}$) | $t_{end}$ (min) | starting mass NRSMA (g) | $\beta_{mass}$ | $m_{seed}$ (mg) | $m_{end}$ (mg) |
|---|---|---|---|---|---|---|---|---|---|---|
| 1 | SIPC | 100 | 23 | 17 | 1.7 | 120 | 21.06 | 1.74 | 50.43 | 2317.71 |
| 2 | SIPC | 100 | 23 | 17 | 1.7 | 60 | 17.34 | 1.43 | 50.20 | 864.42 |
| 3 | SIPC | 100 | 23 | 17 | 1.7 | 60 | 14.79 | 1.22 | 100.19 | 1085.41 |
| 4 | SIPC | 100 | 23 | 17 | 1.7 | 60 | 14.21 | 1.17 | 200.85 | 948.45 |
| 5 | SIPC | 750 | 23 | 17.5 | 0.1 | 180 | 120.36 | 1.32 | 375.47 | 34096.23 |
| 6 | SIPC | 750 | 23 | 17.5 | 0.1 | 60 | 133.13 | 1.47 | 376.80 | 2871.75 |
| 7 | S3PC | 100 | 23 | 17 | 0.07 | 90 | 18.29 | 1.51 | 51.42 | 243.77 |
| 8 | S3PC | 100 | 23 | 17 | 0.05 | 180 | 17.63 | 1.45 | 51.30 | 308.46 |

[a]Seven more experiments were performed, and the results are shown in the Supporting Information.



https://dx.doi.org/10.1021/acs.cgd.0c01236
Cryst. Growth Des. 2020, 20, 7979−7988

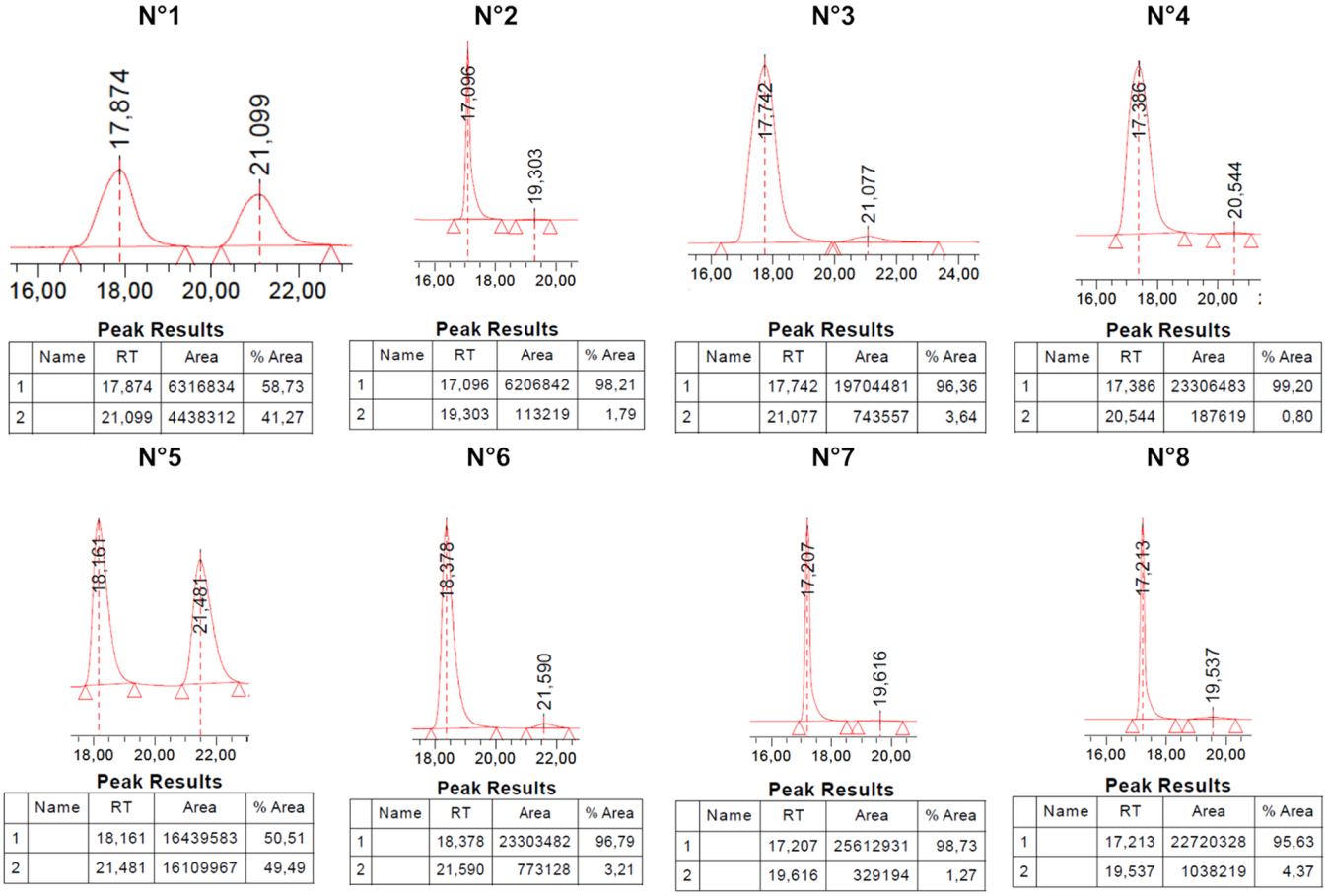


**Figure 10.** View of HPLC data related to each trial. The full chromatograms are presented in Figures S17–S19 in the Supporting Information.

$$\mathrm{Pr}^{\mathrm{NRMA}}(t) = \frac{m_{\mathrm{recovered}}^{\mathrm{NRMA}} - m_{\mathrm{seed}}}{\mathrm{t} \times 0.5 \times m^{\mathrm{NRSMA}}} \quad (2)$$

$$\gamma = \frac{m_{\mathrm{recovered}}^{\mathrm{NRMA}} - m_{\mathrm{seed}}}{0.5 \times (m^{\mathrm{NRSMA}}(\mathrm{T1}) - m^{\mathrm{NRSMA}}(\mathrm{T2}))} \quad (3)$$

$$\beta_{\mathrm{mass}} = \frac{m_{\mathrm{NRSMA(T1)}}}{m_{\mathrm{NRSMA(T2)}}} \quad (4)$$

Results are reported in Table 2.

Preliminary trials revealed a working supersaturation of 6 °C (23–17 °C) and an associated $\beta_{\mathrm{mass}}$ value of 1.2–1.5 to be suitable conditions for the PC process. To get an approximate idea of when to expect the heterogeneous nucleation of the *S* enantiomer on a 100 mL scale, a 120 min trial (no. 1) was performed on sampling the liquid phase. Figure 11A (HPLC data are given in the Supporting Information) shows the solution ee over time, with $t$ = 0 min corresponding to the addition of NRMA seed. The solution ee is shown to increase over time until approximatively 70 min, implying a depletion of the solution in the *R* enantiomer. After this the ee no longer increases, and a decrease clearly sets in after 90 min. A racemic composition of the supernatant solution was obtained once again after 110 min. We expect the heterogeneous nucleation of NSMA therefore to occur about 70 min into the process. Under ideal circumstances, the process needs to be interrupted prior to this nucleation event. As nucleation is stochastic, we decided for the next series of experiments to work with an end time of 60 min which should allow sufficient crystallization of NRMA, while avoiding heterogeneous nucleation of the counter enantiomer.

Three experiments were then repeated under almost identical conditions, with exception of the amount of seed (no. 2, no. 3 and no. 4). These confirm that an enantiopure material is obtained after 60 min of process time (Table 2), which is also highlighted by a single melting endotherm at 115 °C corresponding to the NRMA cocrystal (Figure 9). The presence of traces of the *S* enantiomer is due to the fact that the small amounts recovered did not allow washing the solid. Some mother liquor (containing the *S* enantiomer) is retained by the solid, explaining this presence. Increasing the amount of seed (comparing experiment no. 2 to no. 4) leads to a similar

**Table 2. Values of Purity (Pu), Resolution Index (RI), Productivity (Pr), and Yield ($\gamma$) for the Experiments of Table 1[a]**

| no. | Pu NRMA (%) | RI | Pr NRMA ($10^{-3}$ g g$^{-1}$ min$^{-1}$) | $\gamma$ yield (%) |
|---|---|---|---|---|
| 1 | 49.78 | n/a | n/a | n/a |
| 2 | 98.21 | 15.91 | 1.54 | 27.05 |
| 3 | 96.36 | 9.44 | 2.13 | 32.04 |
| 4 | 99.20 | 4.19 | 1.74 | 25.07 |
| 5 | 50.51 | n/a | n/a | n/a |
| 6 | 96.79 | 6.38 | 0.60 | 11.70 |
| 7 | 98.73 | 3.68 | 0.23 | 8.55 |
| 8 | 95.63 | 4.75 | 0.15 | 11.01 |

[a]Parameters are only calculated for NRMA with purity >90%.



https://dx.doi.org/10.1021/acs.cgd.0c01236
Cryst. Growth Des. 2020, 20, 7979–7988

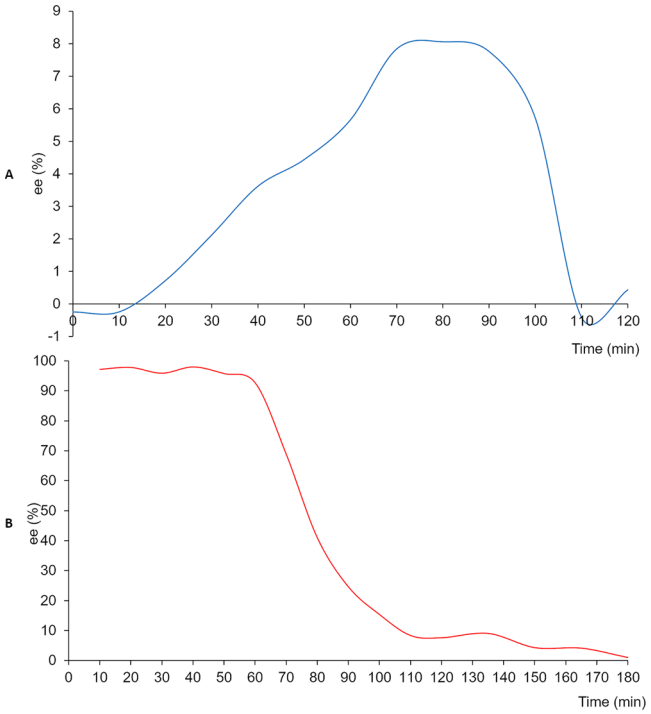


**Figure 11.** (A) NSMA enantiomeric excess in the liquid phase for the 100 mL resolution process. (B) NRMA enantiomeric excess in the solid phase for the 750 mL resolution process. $t$ = 0 min is the addition of the seeds. The HPLC data used to build the diagram are presented in Figures S27−S32 in the Supporting Information.

yield (±30%) and associated productivity ($(1-2) \times 10^{-3}$ g g$^{-1}$ min$^{-1}$). Thecalculated Pr values of $10^{-4}$−$10^{-3}$ g g$^{-1}$ min$^{-1}$ (Table 2) are on the average order of magnitude in comparison with the literature.[38,49] Inherently increasing the amount of seed initially brings more crystals to the process and hence an increase in the rate at which the solution is depleted in $R$ enantiomer. On the basis of these results and as small amounts of seed lead to higher RI values, 50 mg of seed was kept as the parameter for further development.

Upscaling the process to 750 mL, we again carried out a time analysis of the process, this time focusing on the solid phase crystallizing out, as sufficient material could now be recovered for analysis. Figure 11B clearly pinpoints the nucleation of the counter-enantiomer after 60 min of process time and a conglomerate to be obtained after about 100 min. However, one has to be careful comparing this result with that obtained at the 100 mL scale, as for this latter scale, cooling from 23 to 17 °C occurs in a couple of minutes, whereas this takes up to 60 min for the 1 L scale. During this 1 h period (prior to $t$ = 0 of seeding), the solution is in a metastable state and spontaneous nucleation of the counter-enantiomer may occur.

Interrupting the upscaled experiment after 60 min (no. 6) leads to a yield of 2.87 g ($\gamma$ = 11.7%) and a material with high enantiopurity (96.79%), with values of RI comparable to those of the small-scale experiments, albeit showing somewhat lower productivity (Table 3). The 3% counter-enantiomer present in the solid phase (small eutectic endotherm in Figure 9), can once more be explained by poor washing or the potential onset of nucleation of the unseeded enantiomer prior to filtration.

We then set out to verify the resolution using an S3PC mode. In this mode, seeding is performed at the dissolution temperature T1, the highest temperature possible for crystals of NRMA and NSMA to be in equilibrium with a saturated solution. Using a slow cooling ramp, the S3PC mode allows for continuous crystallization of the seed material. Two trials, no. 7 and no. 8, were performed in this mode using cooling rates of 0.067 °C min$^{-1}$ (90 min) and 0.05 °C min$^{-1}$ (180 min), respectively. When T2 was reached, the suspension was filtered. Enantiopure product (98.73%; Figure 10) was observed for the 90 min process (no. 7), whereas the 180 min process (no. 8) showed a slightly more important amount of NSMA present (4.4%), attributed to the potential onset of crystallization of the counter-enantiomer or to insufficient washing. Calorimetric measurements once again show a single melting endotherm at 115 °C corresponding to NRMA (Figure 9). The S3PC mode leads to a lower yield and productivity in comparison to the SIPC mode. This can be attributed to the lower crystallization kinetics, as supersaturation is kept low all along the process. As an advantage, this leads to the nucleation of the counter-enantiomer to be less likely, shown by the longer process times accessible without nucleation of this latter.

Finally, we focused on the feasibility of having a cyclic preferential crystallization, allowing recovering both enantiomers and highlighting a potential toward industrialization of this process. To do so, a six-cycle experiment was performed, starting with a classical SIPC setup as described previously.[51] When the end of the first step was reached, the suspension was filtered and the mother liquor recovered for a second cycle. The recovered mother liquor was fed with an amount of NRSMA conglomerate equivalent to the amount of enantiopure solid that crystallized out during the previous step,

**Table 3. Cyclic Experiment Outcome: $R/S$ Solution Ratio prior to Entrainment, Mass of NRSMA Cocrystal Present in Solution, Mass of Seed Added, Mass of Feed Added at the Onset of Each Step, Mass Recovered in Enantiopure Material, and Purity of This Material[a]**

| Cycle | Ratio R/S | $m_{NRSMA}$ (mg) | $m_{seed}$ (mg) | $m_{feed}$ (mg) | $m_{recov.}$ (mg) | Pu (%) |
|---|---|---|---|---|---|---|
| 1 | 50.45:49.55 | 17338 | 50.18 | / | 368.22 | 98.66 |
| 2 | 48.62:51.38 | 15652 | 51.65 | 371.5 | 685.03 | 97.87 |
| 3 | 51.23:48.77 | 16371 | 50.28 | 685.96 | 488.14 | 97.99 |
| 4 | 48.96:51.04 | 16890 | 51.15 | 490.85 | 310.98 | 98.17 |
| 5 | 50.49:49.51 | 16941 | 50.20 | 311.36 | 139.68 | 98.99 |

[a]Values are given for each step. HPLC and DSC results are shown in Figures S37−S39 in the Supporting Information. Results for the $R$ enantiomer are given in blue and those for the $S$ enantiomer in red.



https://dx.doi.org/10.1021/acs.cgd.0c01236
Cryst. Growth Des. 2020, 20, 7979−7988

keeping an overall constant concentration in mandelic acid. To dissolve the added material, the suspension was slightly heated above T1 until complete dissolution and the solution cooled once again to a temperature of 17 °C (T2). The solution was then seeded at T2 with the desired homochiral seeds. This procedure was then repeated for all of the following steps. First of all, Table 3 shows that each step leads to an enantiopure material, alternating as expected from one enantiomer to the other. In no instance did we encounter nucleation of the counter-enantiomer. Furthermore, addition of racemate at the onset of steps 2−5 leads to a solution that shows a slight excess in one of the two enantiomers, as could be expected. Overall, the six steps of the cycle allowed resolving about 2.36 g of NRSMA. This cycled experiment shows the feasibility of multiple successive entrainment experiments using a racemic feed between each step.

## CONCLUSION

We report the first complete chiral resolution of mandelic acid by preferential cocrystallization. Complementary techniques confirm the existence of a stable mandelic acid−nefiracetam dual-drug cocrystal conglomerate. With this conglomerate as a starting material, a preferential cocrystallization procedure was developed in a seeded isothermal SIPC mode, leading to enantiopure material (up to 98−99%) recovered by the entrainment process with a maximum productivity of $1.74 \times 10^{-3}$ g $g^{-1}$ $min^{-1}$. Follow-up of the solution and solid composition over time showed spontaneous nucleation of the counter-enantiomer to occur only after 70−80 min. The process was shown not only to be easily upscalable but also to lend itself to a cyclic procedure, resolving both enantiomers. Doing so, we were able to resolve 2.4 g of racemic mandelic acid, leading to an enantiopure material. We believe this process not only to have relevant applications on a larger scale (e.g., continuous preferential crystallization) but also to pave the way for other systems which form a conglomerate through cocrystallization.

## ASSOCIATED CONTENT

### Supporting Information

can be found in the Supporting Information as well. This material is available free of charge via the Internet at http://pubs.acs.org." The Supporting Information is available free of charge at https://pubs.acs.org/doi/10.1021/acs.cgd.0c01236.

Additional experiments, crystallographic, calorimetric, and solubility data, and calibration lines and the full chromatograms of each experiment (PDF)

### Accession Codes

CCDC 2023975 and 2032987 contain the supplementary crystallographic data for this paper. These data can be obtained free of charge via www.ccdc.cam.ac.uk/data_request/cif, or by emailing data_request@ccdc.cam.ac.uk, or by contacting The Cambridge Crystallographic Data Centre, 12 Union Road, Cambridge CB2 1EZ, UK; fax: +44 1223 336033.

## AUTHOR INFORMATION


### Corresponding Author

**Tom Leyssens** − *Institute of Condensed Matter and Nanosciences, Université Catholique de Louvain, B-1348 Louvain-la-Neuve, Belgium*; orcid.org/0000-0001-7916-1373; Phone: +32(0)474343884; Email: Tom.leyssens@uclouvain.be

### Authors

**Xavier Buol** − *Institute of Condensed Matter and Nanosciences, Université Catholique de Louvain, B-1348 Louvain-la-Neuve, Belgium*

**Camila Caro Garrido** − *Institute of Condensed Matter and Nanosciences, Université Catholique de Louvain, B-1348 Louvain-la-Neuve, Belgium*

**Koen Robeyns** − *Institute of Condensed Matter and Nanosciences, Université Catholique de Louvain, B-1348 Louvain-la-Neuve, Belgium*

**Nikolay Tumanov** − *Namur Research Institute for Life Sciences (Narilis), Chemistry Department, Université de Namur, B-5000 Namur, Belgium*; orcid.org/0000-0001-6898-9036

**Laurent Collard** − *Institute of Condensed Matter and Nanosciences, Université Catholique de Louvain, B-1348 Louvain-la-Neuve, Belgium*

**Johan Wouters** − *Namur Research Institute for Life Sciences (Narilis), Chemistry Department, Université de Namur, B-5000 Namur, Belgium*

Complete contact information is available at: https://pubs.acs.org/10.1021/acs.cgd.0c01236


### Author Contributions

The manuscript was written through contributions of all authors. All authors have given approval to the final version of the manuscript.


### Funding

The authors thank the "Fonds Européen de Développement Régional" (FEDER) and the "Région Wallonne" in the operational framework Wallonie-2020.EU (Tera4all) for financial support.


### Notes

The authors declare no competing financial interest.

## ACKNOWLEDGMENTS


The authors are grateful to Dr. Celine Rougeot for interesting discussions and advice.


## REFERENCES


(1) Nguyen, L. A.; He, H.; Pham-Huy, C. Chiral drugs: an overview. *Int. J. Biomed. Sci.* **2006**, *2*, 85.

(2) Cahn, R. S.; Ingold, C.; Prelog, V. Specification of molecular chirality. *Angew. Chem., Int. Ed. Engl.* **1966**, *5*, 385−415.

(3) Lin, G.-Q.; You, Q.-D.; Cheng, J.-F. *Chiral drugs: Chemistry and biological action*; Wiley: Hoboken, NJ, 2011.

(4) Blaser, H.-U. Chirality and its implications for the pharmaceutical industry. *Rend. Accad. Naz. Lincei.* **2013**, *24*, 213−216.

(5) Francotte, E.; Lindner, W. *Chirality in drug research*; Wiley-VCH: Weinheim, Germany, 2006; Vol. *33*.

(6) Maier, N. M.; Franco, P.; Lindner, W. Separation of enantiomers: needs, challenges, perspectives. *J. Chromatogr. A* **2001**, *906*, 3−33.

(7) Brooks, W. H.; Guida, W. C.; Daniel, K. G. The significance of chirality in drug design and development. *Curr. Top. Med. Chem.* **2011**, *11*, 760−770.

(8) Blaser, H. U. The chiral pool as a source of enantioselective catalysts and auxiliaries. *Chem. Rev.* **1992**, *92*, 935−952.

(9) Ager, D. J.; Prakash, I.; Schaad, D. R. 1, 2-Amino alcohols and their heterocyclic derivatives as chiral auxiliaries in asymmetric synthesis. *Chem. Rev.* **1996**, *96*, 835−876.

(10) Noyori, R. Asymmetric catalysis: science and opportunities (Nobel Lecture). *Angew. Chem., Int. Ed.* **2002**, *41*, 2008−2022.

(11) Jacobsen, E. N.; Pfaltz, A.; Yamamoto, H. *Comprehensive asymmetric catalysis: Supplement 1*; Springer Science & Business Media: Berlin, Germany, 2003; Vol. *1*.
(12) Chen, C. S.; Fujimoto, Y.; Girdaukas, G.; Sih, C. J. Quantitative analyses of biochemical kinetic resolutions of enantiomers. *J. Am. Chem. Soc.* **1982**, *104*, 7294−7299.
(13) Beesley, T. E.; Scott, R. P. *Chiral chromatography*; Wiley: Chichester, England, 1999.
(14) Kozma, D. *CRC handbook of optical resolutions via diastereomeric salt formation*; CRC Press: New York, 2001.
(15) Harmsen, B.; Leyssens, T. Dual-Drug Chiral Resolution: Enantiospecific Cocrystallization of (S)-Ibuprofen Using Levetiracetam. *Cryst. Growth Des.* **2018**, *18*, 441−448.
(16) Springuel, G.; Leyssens, T. Innovative chiral resolution using enantiospecific co-crystallization in solution. *Cryst. Growth Des.* **2012**, *12*, 3374−3378.
(17) Coquerel, G., Preferential crystallization. In *Novel optical resolution technologies*; Springer: Berlin, Germany, 2006; pp 1−51.
(18) Levilain, G.; Coquerel, G. Pitfalls and rewards of preferential crystallization. *CrystEngComm* **2010**, *12*, 1983−1992.
(19) Srisanga, S.; ter Horst, J. H. Racemic compound, conglomerate, or solid solution: phase diagram screening of chiral compounds. *Cryst. Growth Des.* **2010**, *10*, 1808−1812.
(20) Sakai, K.; Hirayama, N.; Tamura, R. *Novel optical resolution technologies*; Springer: Berlin, Germany, 2007; Vol. *269*.
(21) Galland, A.; Dupray, V.; Berton, B.; Morin-Grognet, S.; Sanselme, M.; Atmani, H.; Coquerel, G. r. Spotting conglomerates by second harmonic generation. *Cryst. Growth Des.* **2009**, *9*, 2713−2718.
(22) Li, W. W.; Spix, L.; De Reus, S. C.; Meekes, H.; Kramer, H. J.; Vlieg, E.; ter Horst, J. H. Deracemization of a racemic compound via its conglomerate-forming salt using temperature cycling. *Cryst. Growth Des.* **2016**, *16*, 5563−5570.
(23) Wacharine-Antar, S.; Levilain, G.; Dupray, V.; Coquerel, G. Resolution of (±)-imeglimin-2, 4-dichlorophenylacetate methanol solvate by preferential crystallization. *Org. Process Res. Dev.* **2010**, *14*, 1358−1363.
(24) Guillot, M.; de Meester, J.; Huynen, S.; Collard, L.; Robeyns, K.; Riant, O.; Leyssens, T. Co-crystallization induced spontaneous deracemization: A general thermodynamic approach to deracemization. *Angew. Chem.* **2020**, *132*, 11399−11402.
(25) Blagden, N.; de Matas, M.; Gavan, P. T.; York, P. Crystal engineering of active pharmaceutical ingredients to improve solubility and dissolution rates. *Adv. Drug Delivery Rev.* **2007**, *59*, 617−630.
(26) Friščić, T.; Jones, W. Benefits of cocrystallisation in pharmaceutical materials science: an update. *J. Pharm. Pharmacol.* **2010**, *62*, 1547−1559.
(27) Sun, C. C. Cocrystallization for successful drug delivery. *Expert Opin. Drug Delivery* **2013**, *10*, 201−213.
(28) Harfouche, L. C.; Brandel, C.; Cartigny, Y.; Petit, S.; Coquerel, G. Resolution by Preferential Crystallization of Proxyphylline by Using Its Salicylic Acid Monohydrate Co-Crystal. *Chem. Eng. Technol.* **2020**, *43*, 1093.
(29) Wang, P.-L.; Wang, H.-B.; Ding, W.-L.; Liu, Z.-Q.; Xing, Z.-T. N-(2, 6-Dimethylphenyl)-2-(2-oxo-1-pyrrolidin-1-yl) acetamide. *Acta Crystallogr., Sect. E: Struct. Rep. Online* **2006**, *62*, o3838−o3839.
(30) Crespi, F. Nefiracetam. Daiichi Seiyaku. *Curr. Opin. Invest. Drugs* **2002**, *3*, 788−793.
(31) Buol, X.; Robeyns, K.; Caro Garrido, C.; Tumanov, N.; Collard, L.; Wouters, J.; Leyssens, T. Improving Nefiracetam Dissolution and Solubility Behavior Using a Cocrystallization Approach. *Pharmaceutics* **2020**, *12*, 653.
(32) Buol, X.; Robeyns, K.; Tumanov, N.; Wouters, J.; Leyssens, T. Identifying, Characterizing, and Understanding Nefiracetam in Its Solid State Forms: A Potential Antidementia Drug. *J. Pharm. Sci.* **2019**, *108*, 3616−3622.
(33) Kesslin, G.; Kelly, K. W. Resolution of racemic mandelic acid. Google Patents: 1982.
(34) Lorenz, H.; Sapoundjiev, D.; Seidel-Morgenstern, A. Enantiomeric mandelic acid system melting point phase diagram and solubility in water. *J. Chem. Eng. Data* **2002**, *47*, 1280−1284.
(35) Sakai, K.; Sakurai, R.; Yuzawa, A.; Kobayashi, Y.; Saigo, K. Resolution of 3-(methylamino)-1-(2-thienyl) propan-1-ol, a new key intermediate for duloxetine, with (S)-mandelic acid. *Tetrahedron: Asymmetry* **2003**, *14*, 1631−1636.
(36) Rougeot, C.; Hein, J. E. Application of continuous preferential crystallization to efficiently access enantiopure chemicals. *Org. Process Res. Dev.* **2015**, *19*, 1809−1819.
(37) Elsner, M. P.; Menéndez, D. F.; Muslera, E. A.; Seidel-Morgenstern, A. Experimental study and simplified mathematical description of preferential crystallization. *Chirality* **2005**, *17*, S183−S195.
(38) Elsner, M. P.; Ziomek, G.; Seidel-Morgenstern, A. Efficient separation of enantiomers by preferential crystallization in two coupled vessels. *AIChE J.* **2009**, *55*, 640−649.
(39) *CrysAlisPro Software System, Ver.1.171.38.41l*; Rigaku Corporation: Oxford, U.K., 2015.
(40) Sheldrick, G. M. Crystal structure refinement with SHELXL. *Acta Crystallogr., Sect. C: Struct. Chem.* **2015**, *71*, 3−8.
(41) Spek, A. L. Structure validation in chemical crystallography. *Acta Crystallogr., Sect. D: Biol. Crystallogr.* **2009**, *65*, 148−155.
(42) Macrae, C. F.; Bruno, I. J.; Chisholm, J. A.; Edgington, P. R.; McCabe, P.; Pidcock, E.; Rodriguez-Monge, L.; Taylor, R.; Streek, J. v. d.; Wood, P. A. Mercury CSD 2.0−new features for the visualization and investigation of crystal structures. *J. Appl. Crystallogr.* **2008**, *41*, 466−470.
(43) Etter, M. C.; MacDonald, J. C.; Bernstein, J. Graph-set analysis of hydrogen-bond patterns in organic crystals. *Acta Crystallogr., Sect. B: Struct. Sci.* **1990**, *46*, 256−262.
(44) Zhang, G. G.; Paspal, S. Y.; Suryanarayanan, R.; Grant, D. J. Racemic species of sodium ibuprofen: Characterization and polymorphic relationships. *J. Pharm. Sci.* **2003**, *92*, 1356−1366.
(45) Ianno, V.; Clevers, S.; Négrier, P.; Dupray, V.; Coquerel, G.; Espeau, P. p-Synephrine enantiomers: binary phase diagram, crystal structure and kinetic stability of a metastable conglomerate monitored by nonlinear optics. *CrystEngComm* **2020**, *22*, 6071.
(46) Schröder, I. Dependence of the solubility of a solid on its melting point. *Z. Phys. Chem.* **1893**, *11*, 449−465.
(47) Van Laar, J. Process of the fusion curves of firm alloys and amalgams. *Arch. Neerl* **1903**, *8*, 264−284.
(48) Klussmann, M.; White, A. J.; Armstrong, A.; Blackmond, D. G. Rationalization and prediction of solution enantiomeric excess in ternary phase systems. *Angew. Chem., Int. Ed.* **2006**, *45*, 7985−7989.
(49) Gendron, F.-X.; Mahieux, J.; Sanselme, M.; Coquerel, G. Resolution of Baclofenium Hydrogenomaleate By Using Preferential Crystallization. A First Case of Complete Solid Solution at High Temperature and a Large Miscibility Gap in the Solid State. *Cryst. Growth Des.* **2019**, *19*, 4793−4801.
(50) Retention times vary from sample to sample, as they significantly depend on the composition of the mobile phase.
(51) In a 100 mL vessel: T1 = 23 °C, cooling rate of 1.7 °C $min^{-1}$, seeding at 17 °C (T2), 50 mg of seeds, process time of 60 min.


https://dx.doi.org/10.1021/acs.cgd.0c01236
*Cryst. Growth Des.* 2020, 20, 7979−7988